Correlation between Polymorphism and Optical Bandwidths in $AgNd(WO_4)_2$

C. Colón,[†] A. Alonso-Medina,[†] F. Fernández,[‡] R. Sáez-Puche,[§] V. Volkov,[||] C. Cascales,*[,||] and C. Zaldo*[,||]

Departamento de Física Aplicada and Departamento de Química Industrial y Polímeros. E.U.I.T. Industrial, Universidad Politécnica de Madrid, Ronda de Valencia 3, 28012 Madrid, Spain, Departamento de Química Inorgánica, Facultad de Ciencias Químicas, Universidad Complutense de Madrid, Avenida Complutense s/n. 28040 Madrid, Spain, and Instituto de Ciencia de Materiales de Madrid, Consejo Superior de Investigaciones Científicas, c/ Sor Juana Inés de la Cruz, 3. Cantoblanco, 28049 Madrid, Spain

Received August 10, 2005. Revised Manuscript Received October 17, 2005

The preparation and characterization of two polymorphic phases of $AgNd(WO_4)_2$ are described. The high-temperature phase of $AgNd(WO_4)_2$ is prepared as a polycrystalline powder and as a single crystal. X-ray diffraction analysis indicates that the crystal has at 300 K the tetragonal symmetry of the space group (SG) $I\bar{4}$ (No. 82), with two independent crystal sites, 2b and 2d, for Nd^{3+} cations and structural disorder around them. The 5 K ground state optical absorption of this tetragonal crystal clearly differs from that corresponding to the monoclinic SG *C*2/*m* (No. 12) ordered phase found in polycrystalline samples prepared below 800 °C. Four times larger bandwidths and a weaker crystal field (CF), that is, lesser CF splitting for all Nd^{3+} $^{2S+1}L_J$ manifolds, are observed for the tetragonal phase. Well-defined S_4 polarization rules have been determined in the tetragonal phase, and then the observed 99 Nd^{3+} energy levels were labeled with the appropriate $\Gamma_{7,8}$ or $\Gamma_{5,6}$ irreducible representations. A detailed Hamiltonian of 26 free ion and CF parameters have been used in the simulation of the phenomenological energy levels and associated wave functions of the $4f^3$ configuration of Nd^{3+} in the tetragonal $AgNd(WO_4)_2$ single crystal, with final $\sigma = 12.6$ cm^{-1}. The validity of the above set of CF parameters and wave functions has been established through the good reproduction of the thermal variation of the measured anisotropic paramagnetic susceptibility χ. As a result of this simulation it is shown that the larger bandwidths of the tetragonal phase contain nonresolved contributions from the two Nd^{3+} sites. A method to control overheating events is proposed on the basis of the nonreversibility of the tetragonal phase into the monoclinic one.

I. Introduction

Polymorphism is the early, best-known structural characteristic of double tungstate (DT) compounds with stoichiometry $XT(WO_4)_2$ [X = alkaline and Ag monovalent cations; T = In, Bi, and rare-earth (RE) trivalent cations]. In fact, depending on the X−T ionic radii relationship and on the temperature of the synthesis (or crystal growth), different phases have been found, including the tetragonal scheelite-type $CaWO_4$, orthorhombic, monoclinic or even triclinic symmetries.[1]

The strong anisotropy (leading to very large optical cross sections) and large lanthanide impurity acceptance of the monoclinic [space group (SG) *C*2/*c*] $KY(WO_4)_2$ and $KGd(WO_4)_2$ single crystals with "ordered" cation environments have promoted their use as efficient laser hosts mainly for Nd^{3+} [2,3] and Yb^{3+} [4] ions. Moreover, these crystals are also known as efficient Raman shifters.[5] These applications have promoted the study of their properties. The DT single crystals with tetragonal crystalline structure ("disordered" materials with regard to their actual cationic distribution) are also known as laser Raman shifters,[6−8] and they received initial attention as laser crystals.[9,10] These early laser experiments evidenced larger bandwidths and lower peak optical cross sections than those observed in the ordered phases prepared

* To whom correspondence should be addressed. E-mail: ccascales@icmm.csic.es (C.Cascales); cezaldo@icmm.csic.es (C.Zaldo).
[†] Departamento de Física Aplicada, Universidad Politécnica de Madrid.
[‡] Departamento de Química Industrial y Polímeros, Universidad Politécnica de Madrid.
[§] Universidad Complutense de Madrid.
[||] Instituto de Ciencia de Materiales de Madrid.

(1) Trunov, V. K.; Efremov, V. A.; Velikodnyj, J. A. *Kristallochimija i svojstva dvojnych molibdatov i vol'framatov*; Nauka: Leningrad, 1986 (in Russian).
(2) Demidovich, A. A.; Shkadarevich, A. P.; Danailov, M. B.; Apai, P.; Gasmi, T.; Gribkovskii, V. P.; Kuzmin, A. N.; Ryabtsev, G. I.; Batay, L. E. *Appl. Phys. B* **1998**, *67*, 11.
(3) Mayor, A.; Langford, N.; Graf, T.; Burns, D.; Ferguson, A. I. *Opt. Lett.* **2002**, *27*, 1478.
(4) Lagatky, A. A.; Kuleshov, N. V.; Mikhailov, V. P. *Opt. Comm.* **1999**, *165*, 71.
(5) Dharmadhikari, J. A.; Dharmadhikari, A. K.; Kumar, G. R. *Appl. Phys. Lett.* **2003**, *83*, 2527.
(6) Kaminskii, A. A.; Nishiota, H.; Kubota, Y.; Ueda, K.; Takuma, H.; Bagaev, S. N.; Pavlyuk, A. A. *Phys. Status Solidi A* **1995**, *148*, 619.
(7) Kaminskii, A. A.; Ueda, K.; Eichler, H. E.; Findeisen, J.; Bagayev, S. N.; Kuznetsov, F. A.; Pavlyuk, A. A.; Boulon, G.: Bourgeois, F. *Jpn. J. Appl. Phys.* **1998**, *37*, L923.
(8) Kaminskii, A. A.; Bagaev, S. N.; Ueda, K.; Nishioka, H.; Kubota, Y.; Chen, X.; Kholov, A. *Jpn. J. Appl. Phys.* **1995**, *34*, L1461.
(9) Zverev, G. M.; Kolodyny, G. Ya. *Sov. Phys. JETP* **1967**, *25*, 217.
(10) Kaminskii, A. A.; Kolodyny, G. Ya; Sergeeva, N. I. *Zh. Prikl. Specktrosc.* **1968**, *9*, 884.

10.1021/cm051789l CCC: $30.25
Published on Web 11/23/2005

at low temperature; therefore, no further laser experiments were pursued with tetragonal DT phases and their properties are not well-known. The interest on the tetragonal DT phases as lasants has been recently renewed by some of the present authors after the achievement of $\Delta\lambda \approx 40$ nm of laser tunability range in a number of DTs doped with Yb[11,12] and the demonstration of sub-100-fs laser pulses in the same crystals.[13] Ultra-short laser pulses and tunability are based on large bandwidths, whose origin must be understood to allow further improvements. The only hypothesis so far advanced to explain the large bandwidth assumes the random distribution of the X−T cations over the single crystallographic 4b site of the centrosymmetric SG $I4_1/a$ of the scheelite structure.[14]

The best known group of DT single crystals obtained as tetragonal phases is based on X = Na.[1,15,16] This is due to the fact that in these systems the phase transition proceeds with weak structural changes, and consequently, crystals can be cooled to room temperature (RT) from the melt without suffering extensive mechanical cracking. The polymorphic transformations of Ag-based DT are complex. The low-temperature α-phase (monoclinic SG $C2/m$, No. 12) → high-temperature β-phase (tetragonal SG $I4_1/a$, No. 88) transformation is easily observed upon heating for all Ce−Lu and Y compounds, but $AgLa(WO_4)_2$ only shows the tetragonal phase.[17,18] Phase transformations observed upon cooling depend on the ionic radius of the T cation. The $\beta \rightarrow \alpha$ transformation is easy only for Er−Lu ions. For Sm−Ho and Y a phase transition to a new monoclinic β' phase is observed upon cooling at about 550 °C.[17,18] For Ce, Pr, and Nd, the $\alpha \rightarrow \beta$ transformation is nearly irreversible; that is, after very long annealing (>50 h to T > 600 °C) only a partial transformation is achieved,[17] and the β phase fully remains for fast (>10 °C/h) cooling rates.

The spectroscopic properties associated to all these phases are scarcely studied. Some preliminary photoluminescence was provided for Eu and Tb,[19] and the Nd^{3+} energy level sequence in low-temperature synthesized polycrystalline $AgNd(WO_4)_2$ has been explained in a monoclinic C_2 local point symmetry.[20]

In the present work we have prepared the two $AgNd(WO_4)_2$ phases. The tetragonal phase was prepared as a polycrystalline powder and as a single crystal grown from its melt by the Czochralski method. Results regarding the structure, the crystal-field (CF) analysis of 5 K polarized optical spectra, and the 2−300 K paramagnetic susceptibility χ of the single crystal are compared to those of the polycrystalline monoclinic $AgNd(WO_4)_2$ phase. As consequence of this study, the broad nature of the optical bands of Nd^{3+} in the tetragonal crystal has been evidenced and its origin discussed. Moreover, applications related to the nonreversibility of the phase transformation are discussed.

II. Experimental Techniques

Polycrystalline $AgNd(WO_4)_2$ phases were prepared by solid-state reactions using stoichiometric amounts of analytical grade Ag_2CO_3, Nd_2O_3, and WO_2. The mixtures were ground and heated in air at temperatures of 670, 800, 900 and 1040 °C, for 6 days to 2 weeks with intermediate regrinding. Crystal structure and purity of the samples were tested by X-ray diffraction analysis always collected at RT. The X-ray diffraction patterns (XRDPs) were performed using a Bruker D-8 diffractometer with Cu Kα radiation, scanning in steps of 0.02° 2θ in the angular range of $10 \leq 2\theta \leq 80$, during 4 s for each step.

Growth of the $AgNd(WO_4)_2$ single crystal was carried out by the Czochralski method. The experimental equipment was described in a previous work.[21] First evidence of the crystal symmetry and orientation were achieved from Laue patterns obtained by using a Siemens Kristalloflex 700 X-ray generator, operating at the Kα emission of a Mo anode. Oriented samples were polished with diamond powders. Unit cell parameters were determined through the analysis by using the Rietveld profile refinement method[22] of the XRDP of a ground portion of the $AgNd(WO_4)_2$ crystal, mixed with W as an internal standard,[23] which was collected by scanning in steps of 0.02° 2θ in the range $10 \leq 2\theta \leq 120$, during 8 s for each step.

The differential thermal analysis (DTA) was made in still air using a simultaneous TG/DTA Stanton equipment, model STA 781. About 72 mg of compound was heated and cooled at a 10 °C/min rate using Al_2O_3 as the reference.

Total reflectance and optical absorption spectra were obtained using a Varian spectrophotometer model CARY 5E. An integrating sphere was used to collect the reflectance at 300 K in the visible and ultraviolet regions. Measurements were carried out as far as 34 000 cm^{-1} in the 5−300 K temperature range. The sample temperature was varied using a He closed cycle cryostat connected to a suitable temperature controller. For single crystals, polarized measurements were made by using a Glan−Taylor polarizer and a depolarizer sheet, while unpolarized measurements were performed for polycrystalline powders dispersed in KBr pellets.

Anisotropic magnetic susceptibility measurements of an oriented $AgNd(WO_4)_2$ crystal were performed in a Quantum Design XL-MPMS SQUID magnetometer, operating at 1000 Oe from 2 to 300 K. Diamagnetic corrections were calculated with conventional values.[24]

(11) Rico, M.; Liu, J.; Griebner, U.; Petrov, V.; Serrano, M. D.; Esteban-Betegón, F.; Cascales, C.; Zaldo, C. *Opt. Express* **2004**, *12*, 5362.
(12) Liu, J.; Cano-Torres, J. M.; Cascales, C.; Esteban-Betegón, F.; Serrano, M. D.; Volkov, V.; Zaldo, C.; Rico, M.; Griebner, U.; Petrov, V.; *Phys. Status Solidi A* **2005**, *202*, R29.
(13) Rivier, S.; Rico, M.; Griebner, U.; Petrov, V.; Serrano, M. D.; Esteban-Betegón, F.; Cascales, C.; Zaldo, C.; Zorn, M.; Weyers, W. Presented at CLEO Europe -EQEC, Münich, 2005; CF4-4-THU.
(14) Kamisnkii, A. A.; Kholov, A.; Klevtsov, P. V.; Khafizov, S. Kh. *Izv. Akad. Nauk SSSR, Neorg. Mater.* **1989**, *25*, 1054.
(15) Rode, E. Ya.; Karpov, V. N.; Ivanova, M. M. *Russ. J. Inorg. Chem.* **1971**, *16*, 905.
(16) Volkov, V.; Rico, M.; Méndez-Blas, A.; Zaldo, C. *J. Phys. Chem. Solids* **2002**, *63*, 95.
(17) Klevtsov, P. V.; Maksin, V. I.; Klevtsova, R. F.; Golub, A. M. *Sov. Phys. Crystallogr.* **1976**, *21*, 430.
(18) Sleight, A. W.; Aykan, K.; Rogers, D. B. *J. Solid State Chem.* **1975**, *13*, 231.
(19) Shi, F.; Meng, J.; Ren, Y. F.; Su, Q. *J. Phys. Chem. Solids* **1998**, *59*, 105.
(20) Colón, C.; Alonso-Medina, A.; Montero, J.; Fernández, F.; Cascales, C. *J. Chem. Phys.* **2003**, *119*, 13007. The polycrystalline low-temperature $AgNd(WO_4)_2$ sample studied in this work was erroneously described as a tetragonal scheelite-like phase.
(21) Volkov, V.; Zaldo, C. *J. Cryst. Growth* **1999**, *206*, 60.
(22) Roisnel, T.; Rodríguez-Carvajal J.; *WinPLOTR*; http://www-llb.cea.fr/fullweb/winplotr/winplotr.htm (plotr@llb.saclay.cea.fr).
(23) Parrish, W. *Acta Crystallogr.* **1960**, *13*, 838.
(24) Boudreaux, A.; Mulay, L. N.; *Theory and Applications of Molecular Paramagnetism*; Wiley: New York, 1976; p 494.

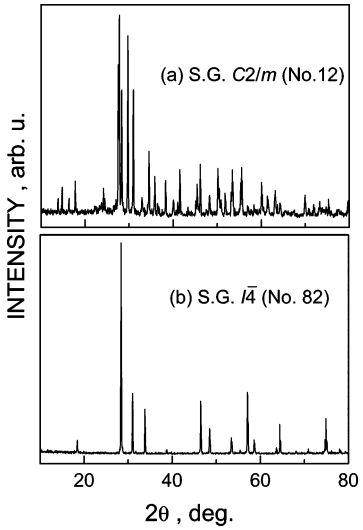

Figure 1. RT XRDP of $AgNd(WO_4)_2$ phases. (a) Monoclinic SG *C*2/*m* obtained by 670 °C annealing for 2 weeks. (b) Tetragonal SG $I\bar{4}$ obtained by 1040 °C annealing for 6 days.

III. Results and Discussion

Synthesis of Polycrystalline $AgNd(WO_4)_2$ Samples. Samples synthesized at 670 °C for 2 weeks show the characteristic features of a low symmetry phase, whereas those corresponding to samples prepared at higher than 800 °C temperature appear to be very similar to those observed for the grown crystal described later. Whereas the preparation of well-crystallized powders of the tetragonal phase can be carried out with annealing times of a few days (typically 2−6 days, depending on the annealing temperature), synthesizing the monoclinic phase requires a longer lasting thermal treatment (∼2 weeks). All prepared samples appeared free of other crystalline phases. Figure 1 shows a comparison between XRDPs for both phases.

The careful XRDP analysis of samples prepared by low-temperature annealing indicates that they are isostructural to the monoclinic α-phase, SG *C*2/*m* (No. 12), described for $AgEr(WO_4)_2$ as a representative of the $AgRE(WO_4)_2$ family.[17]

Crystal Growth of $AgNd(WO_4)_2$. The polycrystalline powder synthesized above 800 °C was used as starting material for the Czochralski crystal growth. This powder was melted in a Pt crucible, and the crystal growth seeded with Pt wire. The pulling and rotating speeds were 1 mm/h and 5 rpm, respectively. The boule was cooled to RT at about 10 °C/h until 500 °C and at 30 °C/h in the 500−20 °C range. The crystallized boule showed a deep violet color, and a part of it exhibited good transparency, with few macroscopic defects. Only this latter part was used in the current study.

The DTA of the crystal (Figure 2) indicated congruent fusion at 1164 °C, and no new features upon cooling have been observed. The absence of new DTA peaks upon cooling confirms the unfavorable character of the tetragonal $\beta \rightarrow$ monoclinic α transformation. Therefore, the tetragonal phase achieved after the melt solidification is quenched at RT.

XRDP of the ground $AgNd(WO_4)_2$ crystal appears to be similar to that described for the tetragonal β'-phase of $AgRE(WO_4)_2$.[17] The Rietveld profile refinement, Figure 3, was currently performed in the tetragonal SG $I\bar{4}$ (No. 82), using starting values of the unit cell and positional parameters

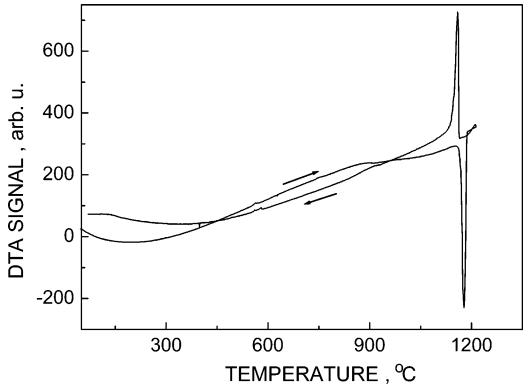

Figure 2. DTA of the $AgNd(WO_4)_2$ single crystal obtained by the Czochralski method.

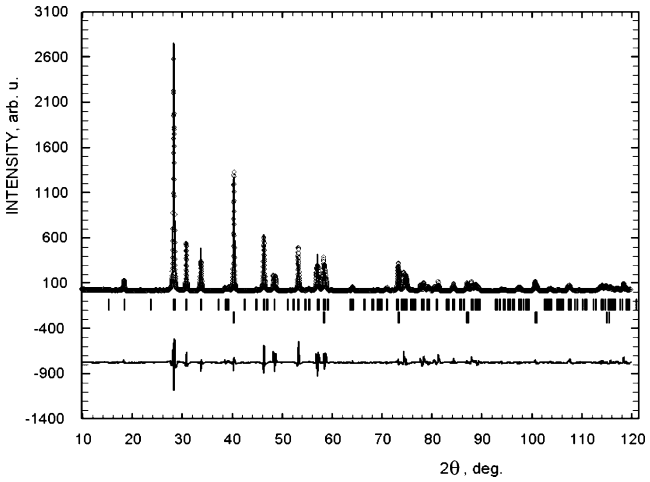

Figure 3. RT XRDP of a mixture of ground $AgNd(WO_4)_2$ single crystal and W phases. Observed results (circles), $I\bar{4}$ Rietveld calculated (continuous line) and difference (line at the bottom). Vertical marks correspond to the Bragg reflections of $AgNd(WO_4)_2$ (top row) and W (bottom row).

previously reported for the isostructural $LiYb(MoO_4)_2$ single crystal,[25] yielding final crystal cell values of $a = 5.3162(2)$ and $c = 11.6167(7)$ Å.

Crystal Structure of Monoclinic *C*2/*m* and Tetragonal $I\bar{4}$ $AgNd(WO_4)_2$ Phases. The low-temperature, monoclinic *C*2/*m* $AgNd(WO_4)_2$ phase contains four kinds of coordination polyhedra: Nd^{3+} cations have a single coordination to eight oxygens, whereas the Ag^+ and the two types of W^{6+} cations have environments of six oxygens. Every two NdO_8 polyhedra are associated by sharing edges along the *b* axis, forming isolated Nd_2O_{14} units, which are aligned in rows parallel to *b*, linked between them through $W2O_6$ and $W1O_6$ groups in *a* and *c* directions, respectively. Figure 4, left, displays a perspective along the [110] direction of this structure.

On the other hand, the crystal structure of the high-temperature, tetragonal $I\bar{4}$ phase of $AgNd(WO_4)_2$ contains two types of Nd/AgO_8 distorted square antiprisms and $W1O_4$ and $W2O_4$ tetrahedral groups. Along the *a* and *b* directions the structure is built of parallel chains of alternate, edge-sharing Nd/AgO_8 and WO_4 polyhedra, of only one type in each row, and in the *c* direction Nd/AgO_8 polyhedra from two different consecutive chains are linked through a

(25) Volkov, V.; Cascales, C.; Kling, A.; Zaldo, C. *Chem. Mater.* **2005**, *17*, 291.

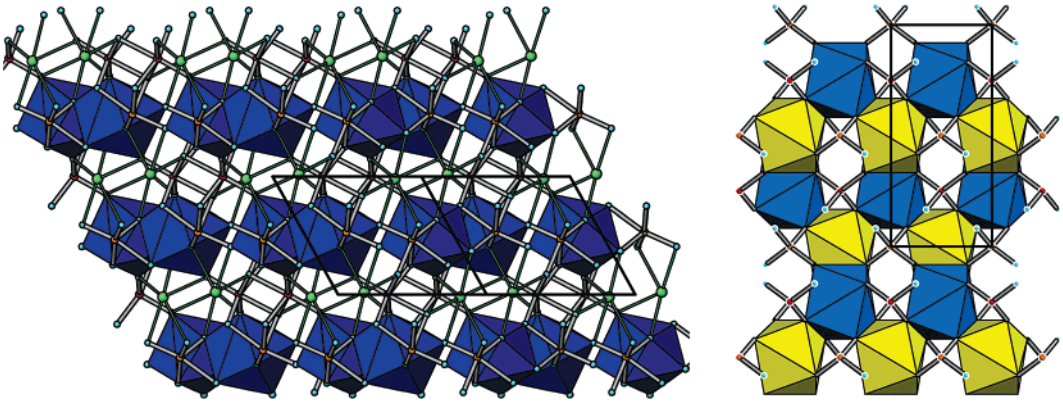

Figure 4. Left: view along the [110] direction of the structure of the monoclinic *C*2/*m* $AgNd(WO_4)_2$ phase. NdO_8 are the blue polyhedra, and green, red, and cyan spheres represent Ag, W, and O ions, respectively. Right: the *ac* perspective of the structure of tetragonal $I\bar{4}$. Yellow and blue polyhedra correspond to NdO_8 for the 2b and 2d lattice sites, and red and cyan spheres represent W and O ions, respectively.

common face, forming $(Ag/Nd)_2O_{12}$ dimeric units; see Figure 4, right.

Some features must be retained from the comparison between the monoclinic and tetragonal structures of $AgNd(WO_4)_2$. In the first case Nd^{3+} occupies only one C_{2v} crystallographic site, while in the noncentrosymmetric $I\bar{4}$ host Nd^{3+} and Ag^+ cations are sharing, with nearly statistical occupation, two S_4 crystal sites, 2b and 2d. Accordingly, these phases can be qualified respectively as "ordered" or "disordered" with regards to the actual cationic environment(s) around the Nd^{3+} site(s). Furthermore, both S_4 NdO_8 square antiprisms in the disordered tetragonal phase are highly regular polyhedra, contrasting with the C_{2v} NdO_8 polyhedron, which is characterized by a larger distribution of Nd−O distances, with one of them clearly shorter than the average value. These two criteria, the ordered or disordered nature of the structure of the crystal phase and the distortion degree of the corresponding NdO_8 polyhedra, will lead the discussion on the observed spectroscopic properties in the following sections.

Optical Reflectance and Color. The colors of the phases achieved by low- (670 °C) and high- (>800°C) temperature annealing are quite different and depend on the illumination conditions. Figure 5 shows the colors observed under sunlight, a quartz halogen lamp, and a UV-filtered fluorescent lamp. In the first two cases, Figure 5a, the light contains a significant UV intensity giving rise to a pale gray color for the low-temperature phase and a deep purple color for the high-temperature phase. When the UV emission is eliminated from the irradiation source these colors render into pale green and grayish blue, respectively, Figure 5b.

Figure 6 shows a comparison of the RT total reflectance of both phases. The Nd^{3+} optical absorption bands induce well-defined reduction in the reflectance. The more obvious differences between the reflectance spectra of the two phases are the narrower character of the features associated to the monoclinic phase and the apparent higher reflectance of the tetragonal phase in the 450−300 nm region. However, this latter difference must be taken with caution because Nd^{3+} fluorescence can be excited in this region giving rise to red emissions (λ = 600, 650−700 nm) from the de-excitation of $^4G_{7/2}$, $^4G_{5/2}$, and $^4F_{9/2}$ to the $^4I_{11/2}$, and $^4I_{9/2}$ Nd^{3+} states. This fluorescence can contribute to the observed color and eventually enhance the light intensity collected by the integrating sphere. So the actual color seen by the eye is a

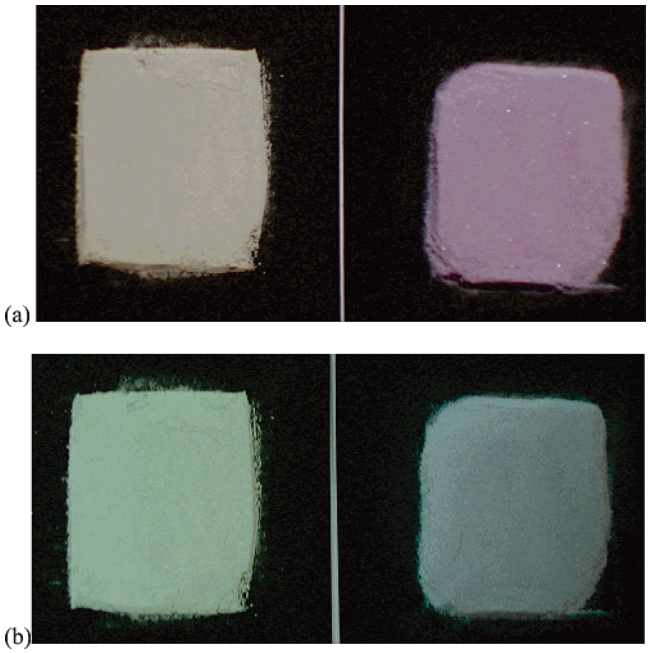

Figure 5. Colors of the monoclinic (left) and tetragonal (right) $AgNd(WO_4)_2$ phases under different illumination conditions. (a) Sun and halogen quartz lamp light. (b) UV-filtered fluorescent lamp.

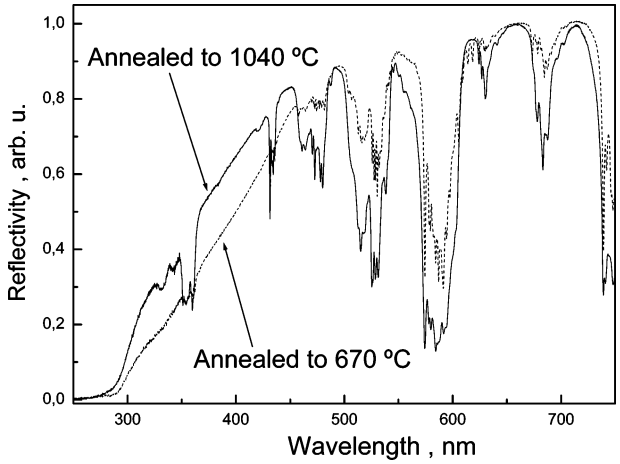

Figure 6. RT total reflectance of $AgNd(WO_4)_2$ phases. Monoclinic phase prepared by 670 °C annealing, dotted line. Tetragonal phase prepared by 1040 °C annealing, continuous line.

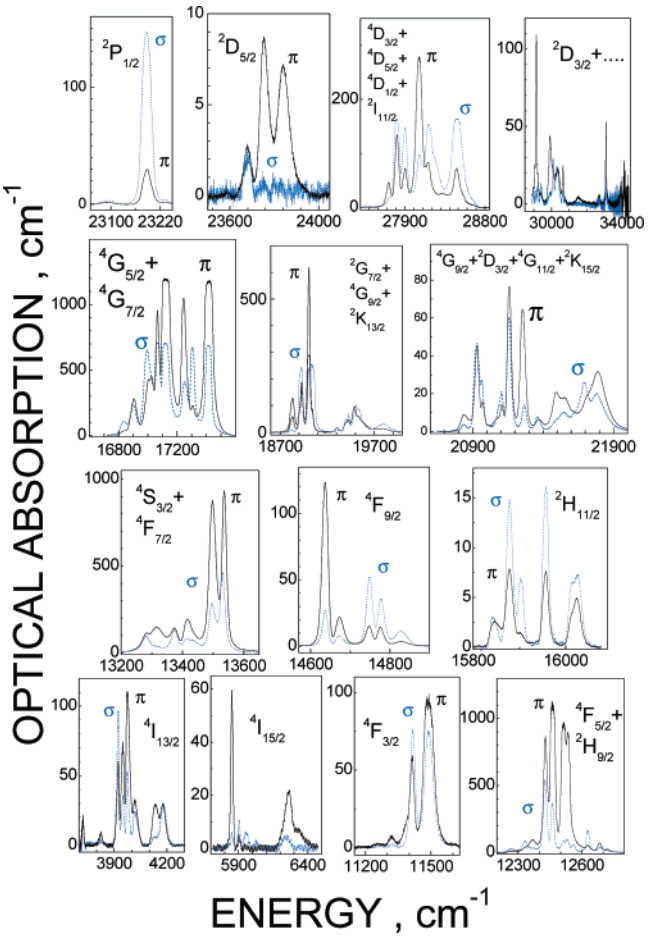

Figure 7. GSA (5 K) of tetragonal $AgNd(WO_4)_2$ single crystal, [Nd] = 6.1×10^{21} cm^{-3}. π spectra, continuous line. σ spectra, dashed line.

combination of the reflectance and fluorescence properties of the material. Whatever this combination, the RT colors of the tetragonal and monoclinic phases are easy to distinguish. This provides a method to evidence the achievement of a temperature level in a process.

For the $AgNd(WO_4)_2$ compound the threshold temperature required to induce its permanent color change is 800 °C; however, other DT compounds based on different alkali ions (K, Rb, Cs) and the corresponding double molybdates can be envisaged to select specific transformation temperatures. All these compounds melt at a temperature 200−400 °C higher than that corresponding irreversible polymorphic transformation, providing an acceptable operating overheating temperature range.

Optical Absorption Spectra. At low enough temperature it is expected that transitions in the optical absorption spectrum of Nd^{3+} originate only from the lowest Stark component of the $^4I_{9/2}$ ground-state manifold, given that other excited levels are not populated.

Figure 7 shows an overview of the 5 K polarized ground-state optical absorption (GSA) spectra for the tetragonal $AgNd(WO_4)_2$ single crystal. According to the crystallographic model both optical Nd^{3+} centers have $\bar{4}$ inversion axes parallel to the *c* crystal axis, and, thus, experimental spectra have been labeled σ ($E \perp c$; $B \parallel c$) or π ($E \parallel c$; $B \perp c$). *J* manifolds of the $4f^3$ configuration of Nd^{3+} are split in $J + 1/2$ Stark levels, Kramers doublets in this case. These measurements give the position of the Stark levels from $^4I_{13/2}$ up to $^2H1_{11/2}$. Even at this low temperature, spectral line profiles of all observed multiplets exhibit a significant broadening, and the individual contributions of the 2b and 2d sites of Nd^{3+} are not resolved. Despite this broadening, Figure 7 shows that observed Nd^{3+} transitions possess polarization characteristics compatible with S_4 symmetry selection rules, and we can reasonably perform the CF analysis assuming an average S_4 potential.

Energy level positions of the ground $^4I_{9/2}$ manifold have been derived from the evolution of nonpolarized $^4I_{9/2} \rightarrow {}^2P_{1/2}$ transitions at increasing temperatures, not shown for the sake of brevity.

The energy level sequence and polarization character of the transitions generally resemble those of Nd^{3+} in $NaBi(WO_4)_2$,[26] but as a result of the high Nd concentration in the $AgNd(WO_4)_2$ single crystal ([Nd]= 6.1×10^{21} cm^{-3}) even transitions with very weak oscillator strength, like $^2H_{11/2}$, can be now observed. This leads to the observation of more energy levels than those found for Nd^{3+} in $NaBi(WO_4)_2$, 99 versus 85, respectively.

Table 1 includes all observed Nd^{3+} energy levels in the $AgNd(WO_4)_2$ single crystal, along with the line widths (full width at half-maximum, fwhm) ΔE_0 of selected GSA transitions.

It is noteworthy that 5 K nonpolarized GSA spectra of polycrystalline samples synthesized by thermal treatments at $T > 800$ °C are found to be nearly identical to the $(2\sigma + \pi)/3$ average spectra of the above tetragonal single crystal. This is clearly seen by analyzing the $^4F_{9/2}$ and $^4F_{3/2}$ absorption spectra, which as shown in Figure 7 are sensitive to the polarization. When these polarized spectra in the crystal are averaged as indicated above, the relative intensity of the band components of $^4F_{9/2}$ (or $^4F_{3/2}$) are similar to those found using powder; see Figure 8b,c. As previously indicated, given the thermal region of stability of the disordered tetragonal phase, these prepared polycrystalline samples are isostructural to the grown single crystal. Obviously, the determination of the polarization character of a given transition, that is, more complete information on irreducible representations (IR) of the observed energy levels, can be derived only with measurements on the $AgNd(WO_4)_2$ single crystal.

On the other hand, the 5 K GSA nonpolarized spectra observed in the present work for $AgNd(WO_4)_2$ polycrystalline samples synthesized at 670 °C are identical to those reported in a previous work[20] and, as already discussed, correspond to the *C*2/*m* monoclinic structure. In this low-temperature phase, only one Nd^{3+} center exists, and consequently the $^4I_{9/2} \rightarrow {}^2P_{1/2}$ transition has a unique and narrow (fwhm $\Delta E = 7$ cm^{-1}) band at 23 160 cm^{-1}; see Figure 8a.

More differences between the optical absorption spectra of the high-temperature tetragonal phase (the single crystal and the polycrystalline sample synthesized at 1040 °C) and the low (670 °C) temperature monoclinic $AgNd(WO_4)_2$ phase are also evidenced in Figure 8. The most relevant differences found are the larger bandwidths for the tetragonal phase,

(26) Méndez-Blas, A.; Volkov, V.; Cascales, C.; Zaldo, C. *J. Alloys Compd.* **2001**, *323*, 315.

Table 1. 5 K Experimental (E_0) and S_4 Calculated (E_c) Energy Levels (cm^{-1}) of Nd^{3+} in the $AgNd(WO_4)_2$ Single Crystal[a]

$^{2S+1}L_J$	||	IR	E_0	E_c	ΔE_0	ΔE_c	$^{2S+1}L_J$	||	IR	E_0	E_c	ΔE_0	ΔE_c
$^4I_{9/2}$	σ	$\Gamma_{7,8}$	0	−5			$^4G_{11/2}$	$\sigma\pi$	$\Gamma_{5,6}$	21 369	21 377		16
	σ	$\Gamma_{7,8}$	96	101		14	$^2K_{15/2}$	$\sigma\pi$	$\Gamma_{5,6}$	21 493	21 480		32
	$\sigma\pi$	$\Gamma_{5,6}$	162	163		0	$^2K_{15/2}$		$\Gamma_{7,8}$		21 523		39
	$\sigma\pi$	$\Gamma_{5,6}$	240	231		20	$^4G_{11/2}$	σ	$\Gamma_{7,8}$	21 546	21 540		38
	σ	$\Gamma_{7,8}$	410	424		51	$^2K_{15/2}$	$\sigma\pi$	$\Gamma_{5,6}$	21 555	21 553		46
$^4I_{11/2}$		$\Gamma_{7,8}$		1959		13	$^2K_{15/2}$		$\Gamma_{7,8}$		21 569		24
		$\Gamma_{7,8}$		2001		14	$^2K_{15/2}$	σ	$\Gamma_{7,8}$	21 629	21 615		40
		$\Gamma_{5,6}$		2001		13	$^2K_{15/2}$		$\Gamma_{5,6}$		21 624		28
		$\Gamma_{5,6}$		2042		14	$^4G_{11/2}$		$\Gamma_{7,8}$		21 658		44
		$\Gamma_{5,6}$		2158		34	$^4G_{11/2}$	$\sigma\pi$	$\Gamma_{5,6}$	21 696	21 679		45
		$\Gamma_{7,8}$		2187		39	$^2K_{15/2}$	$\sigma\pi$	$\Gamma_{5,6}$	21 790	21 790		44
$^4I_{13/2}$	σ	$\Gamma_{7,8}$	3923	3947	13	11	$^2K_{15/2}$		$\Gamma_{7,8}$		21 800		43
	$\sigma\pi$	$\Gamma_{5,6}$	3948	3918	19	10	$^2P_{1/2}$	σ	$\Gamma_{7,8}$	23 188	23 186	26	22
	$\sigma\pi$	$\Gamma_{5,6}$	3975	3969	21	11	$^2D1_{5/2}$	σ	$\Gamma_{7,8}$	23 680	23 697		25
	σ	$\Gamma_{7,8}$	4017	4002	32	9		$\sigma\pi$	$\Gamma_{5,6}$	23 753	23 749		24
	$\sigma\pi$	$\Gamma_{5,6}$	4134	4132	37	28		$\sigma\pi$	$\Gamma_{5,6}$	23 839	23 839		26
	$\sigma\pi$	$\Gamma_{5,6}$	4176	4169	30	40	$^2P_{3/2}$		$\Gamma_{7,8}$		26 072		20
	σ	$\Gamma_{7,8}$	4179	4171	36	42			$\Gamma_{5,6}$		26 144		20
$^4I_{15/2}$	$\sigma\pi$	$\Gamma_{5,6}$	5852	5864	19	1	$^4D_{3/2}$	$\sigma\pi$	$\Gamma_{5,6}$	27 809	27 784		1
	$\sigma\pi$	$\Gamma_{5,6}$	5902	5914	16	6		σ	$\Gamma_{7,8}$	27 900	27 893		14
	σ	$\Gamma_{7,8}$	5958	5970	23	6	$^4D_{5/2}$	$\sigma\pi$	$\Gamma_{5,6}$	28 066	28 069		32
	σ	$\Gamma_{7,8}$	6025	6026		8	$^4D_{5/2}$	$\sigma\pi$	$\Gamma_{5,6}$	28 160	28 172		26
	σ	$\Gamma_{7,8}$	6243	6243	55	42		σ	$\Gamma_{7,8}$	28 234	28 243		36
	$\sigma\pi$	$\Gamma_{5,6}$	6265	6269	47	43	$^4D_{1/2}$	σ	$\Gamma_{7,8}$	28 485	28 505		24
		$\Gamma_{7,8}$		6304		43	$^2I_{11/2}$	$\sigma\pi$	$\Gamma_{5,6}$	28 978	28 977		2
		$\Gamma_{5,6}$		6334		56		σ	$\Gamma_{7,8}$	29 053	29 076		4
$^4F_{3/2}$	σ	$\Gamma_{7,8}$	11 415	11 410	24	20		$\sigma\pi$	$\Gamma_{5,6}$	29 145	29 145		2
	$\sigma\pi$	$\Gamma_{5,6}$	11 485	11 469	47	20		σ	$\Gamma_{7,8}$	29 232	29 236		12
$^4F_{5/2}$	σ	$\Gamma_{7,8}$	12 426	12 416		14		σ	$\Gamma_{7,8}$	29 404	29 415		30
	$\sigma\pi$	$\Gamma_{5,6}$	12 462	12 454		10		$\sigma\pi$	$\Gamma_{5,6}$		29 420		30
		$\Gamma_{5,6}$	12 514	12 523	17	21	$^2L_{15/2}$	σ	$\Gamma_{7,8}$		29 838		29
$^2H2_{9/2}$	$\sigma\pi$	$\Gamma_{5,6}$	12 534	12 548	18	8	$^2L_{15/2}$	$\sigma\pi$	$\Gamma_{5,6}$	29 921	29 930		16
	σ	$\Gamma_{7,8}$	12 558	12 556	13	26	$^2L_{15/2}$	$\sigma\pi$	$\Gamma_{5,6}$		30 012		19
	σ	$\Gamma_{7,8}$	12 628	12 636	16	16	$^4D_{7/2}$	σ	$\Gamma_{7,8}$		30 052		23
	$\sigma\pi$	$\Gamma_{5,6}$	12 684	12 667	20	32	$^2L_{15/2}$	σ	$\Gamma_{7,8}$	30 092	30 080		27
	σ	$\Gamma_{7,8}$	12 717	12 725	25	31	$^2L_{15/2}$	σ	$\Gamma_{7,8}$		30 137		29
$^4F_{7/2}$	σ	$\Gamma_{7,8}$	13 374	13 383	21	17	$^4D_{7/2}$	$\sigma\pi$	$\Gamma_{5,6}$		30 148		18
$^4F_{7/2}$	$\sigma\pi$	$\Gamma_{5,6}$	13 416	13 416	18	17	$^4D_{7/2}$	σ	$\Gamma_{7,8}$	30 319	30 308		16
$^4S_{3/2}$	σ	$\Gamma_{7,8}$	13 435	13 435	21	20	$^4D_{7/2}$	$\sigma\pi$	$\Gamma_{5,6}$		30 337		27
$^4S_{3/2}$	$\sigma\pi$	$\Gamma_{5,6}$		13 442		21	$^2L_{15/2}$	σ	$\Gamma_{7,8}$		30 357		28
$^4F_{7/2}$	$\sigma\pi$	$\Gamma_{5,6}$	13 498	13 517	25	31	$^2L_{15/2}$	$\sigma\pi$	$\Gamma_{5,6}$		30 371		32
$^4F_{7/2}$	σ	$\Gamma_{7,8}$	13 536	13 532	17	29	$^2I_{13/2}$	$\sigma\pi$	$\Gamma_{5,6}$		30 407		35
$^4F_{9/2}$	$\sigma\pi$	$\Gamma_{5,6}$	14 637	14 635	17	14		σ	$\Gamma_{7,8}$		30 497		3
	σ	$\Gamma_{7,8}$	14 673	14 666	22	15		$\sigma\pi$	$\Gamma_{5,6}$		30 506		11
	σ	$\Gamma_{7,8}$	14 748	14 765	20	29		σ	$\Gamma_{7,8}$		30 627		10
	$\sigma\pi$	$\Gamma_{5,6}$	14 776	14 772	18	27		$\sigma\pi$	$\Gamma_{5,6}$	30 661	30 649		20
		$\Gamma_{7,8}$		14 839		28		σ	$\Gamma_{7,8}$		30 774		30
$^2H2_{11/2}$	σ	$\Gamma_{7,8}$	15 843	15 858	14	8		$\sigma\pi$	$\Gamma_{5,6}$		30 778		39
	$\sigma\pi$	$\Gamma_{5,6}$	15 878	15 890	14	11	$^2L_{17/2}$	σ	$\Gamma_{7,8}$		31 303		31
	σ	$\Gamma_{7,8}$	15 902	15 911	12	15		σ	$\Gamma_{7,8}$		31 412		25
	$\sigma\pi$	$\Gamma_{5,6}$	15 956	15 955	14	20		$\sigma\pi$	$\Gamma_{5,6}$		31 495		21
	σ	$\Gamma_{7,8}$	16 015	16 005	17	27		$\sigma\pi$	$\Gamma_{5,6}$		31 572		29
	$\sigma\pi$	$\Gamma_{5,6}$	16 025	16 033	21	27		σ	$\Gamma_{7,8}$		31 621		30
$^4G_{5/2}$	$\sigma\pi$	$\Gamma_{5,6}$	17 025	17 019	20	1		σ	$\Gamma_{7,8}$		31 680		35
	σ	$\Gamma_{7,8}$	17 066	17 062	21	17		$\sigma\pi$	$\Gamma_{5,6}$		31 686		26
	$\sigma\pi$	$\Gamma_{5,6}$	17 120	17 129		18		σ	$\Gamma_{7,8}$		31 825		35
$^4G_{7/2}$	$\sigma\pi$	$\Gamma_{5,6}$	17 243	17 237	31	19		$\sigma\pi$	$\Gamma_{5,6}$		31 831		41
$^4G_{7/2}$	σ	$\Gamma_{7,8}$	17 251	17 233	38	24	$^2H1_{9/2}$	σ	$\Gamma_{7,8}$		32 596		23
$^4G_{7/2}$	σ	$\Gamma_{7,8}$	17 303	17 300	26	28		$\sigma\pi$	$\Gamma_{5,6}$	32 681	32 680		29
$^4G_{7/2}$	$\sigma\pi$	$\Gamma_{5,6}$	17 411	17 422		46		σ	$\Gamma_{7,8}$		32 680		23
$^2G_{7/2}$	σ	$\Gamma_{7,8}$	18 907	18 904	22	2		$\sigma\pi$	$\Gamma_{5,6}$	32 749	32 745		37
$^2G_{7/2}$	$\sigma\pi$	$\Gamma_{5,6}$	18 927	18 929	24	8			$\Gamma_{7,8}$		32 777		34
$^2G_{7/2}$	$\sigma\pi$	$\Gamma_{5,6}$	19 003	18 027	24	14	$^2D2_{3/2}$	$\sigma\pi$	$\Gamma_{5,6}$	33 107	33 122		20
$^2G_{7/2}$	σ	$\Gamma_{7,8}$	19 043	19 050		16		σ	$\Gamma_{7,8}$		33 211		27
$^4G_{9/2}$	σ	$\Gamma_{7,8}$	19 314	19 331		5	$^2H1_{11/2}$	$\sigma\pi$	$\Gamma_{5,6}$		33 915		12
$^4G_{9/2}$	$\sigma\pi$	$\Gamma_{5,6}$	19 394	19 390	24	12	$^2D2_{5/2}$	$\sigma\pi$	$\Gamma_{5,6}$	33 959	33 958		24
$^4G_{9/2}$	σ	$\Gamma_{7,8}$	19 423	19 424	24	20	$^2D2_{5/2}$	σ	$\Gamma_{7,8}$		33 981		12
$^4G_{9/2}$	$\sigma\pi$	$\Gamma_{5,6}$	19 491	19 498	36	29	$^2H1_{11/2}$	$\sigma\pi$	$\Gamma_{5,6}$		34 054		32
$^4G_{9/2}$	σ	$\Gamma_{7,8}$	19 505	19 506	36	29	$^2H1_{11/2}$	σ	$\Gamma_{7,8}$		34 074		30
$^2K_{13/2}$	$\sigma\pi$	$\Gamma_{5,6}$	19 530	19 507	42	26	$^2H1_{11/2}$	$\sigma\pi$	$\Gamma_{5,6}$		34 104		37
$^2K_{13/2}$		$\Gamma_{7,8}$		19 533		30	$^2D2_{5/2}$	σ	$\Gamma_{7,8}$		34 132		35
$^2K_{13/2}$		$\Gamma_{5,6}$		19 552		37	$^2H1_{11/2}$	$\sigma\pi$	$\Gamma_{5,6}$		34 240		55
$^2K_{13/2}$		$\Gamma_{5,6}$		19 565		21	$^2H1_{11/2}$	σ	$\Gamma_{7,8}$		34 243		44
$^2K_{13/2}$		$\Gamma_{7,8}$		19 576		29							
$^2K_{13/2}$	σ	$\Gamma_{7,8}$	19 804	19 804	60	43							
$^2K_{13/2}$	$\sigma\pi$	$\Gamma_{5,6}$		19 813		38							
$^2G1_{9/2}$	$\sigma\pi$	$\Gamma_{5,6}$	20 929	20 924	24	0							
$^2G1_{9/2}$	σ	$\Gamma_{7,8}$	20 966	20 952		11							
$^2G1_{9/2}$		$\Gamma_{5,6}$		20 974		2							
$^2G1_{9/2}$		$\Gamma_{7,8}$		20 979		4							
$^2G1_{9/2}$	σ	$\Gamma_{7,8}$	21 084	21 074		12							
$^2D1_{3/2}$	σ	$\Gamma_{7,8}$	21 105	21 106	28	16							
$^2D1_{3/2}$	$\sigma\pi$	$\Gamma_{5,6}$	21 158	21 126	30	12							
$^4G_{11/2}$	$\sigma\pi$	$\Gamma_{5,6}$	21 254	21 262		1							

[a] || indicates the polarization of the observed band, and IR represents the corresponding irreducible representation. ΔE_0 is the observed fwhm for some selected OA transitions. The energy difference between equivalent energy levels for the 2b and 2d S_4 sites, calculated with SOM, appears as ΔE_c. Reduced $U^4/4$ tables have been utilized for the $^2H2_{11/2}$ multiplet.

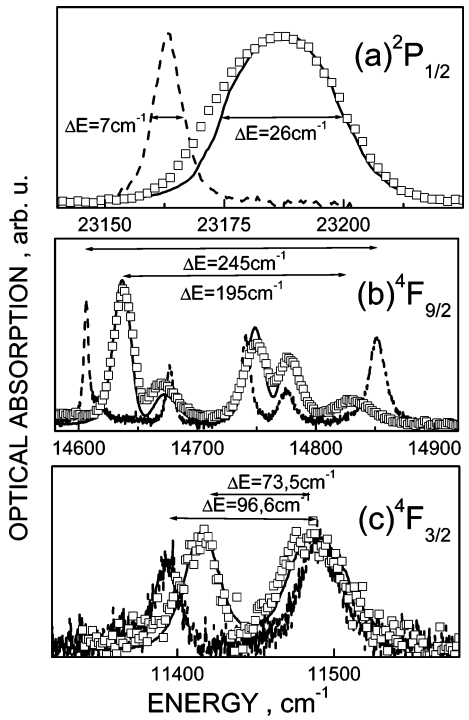

Figure 8. Comparison of the 5 K Nd^{3+} GSA of tetragonal and monoclinic phases of $AgNd(WO_4)_2$. Polycrystalline tetragonal phase, squares. Polycrystalline monoclinic phase, dashed line. Spectra of the tetragonal single crystal, continuous line. (a) σ spectra; (b and c) $(2\sigma + \pi)/3$ average spectrum.

typically up to four times that found for the monoclinic one, and the more intense CF splitting of all manifolds for the monoclinic phase, as can be clearly observed for multiplets depicted in Figure 8b,c.

To quantify the Nd^{3+} energy level differences between the 2b and the 2d sites in the tetragonal phase we shall complete the following steps: (a) calculation of an optimized set of phenomenological free ion (FI) and CF parameters to reproduce the energy level sequence of an average Nd^{3+} center; (b) validation of the latter set and associated wave functions by independent measurements of the paramagnetic susceptibility; (c) simulation of individual subsets of CF parameters for the 2b and 2d sites by using the simple overlap model, SOM; and (d) calculation of separate energy level sequences for these sites by using common FI parameters but CF parameters specific for each site. The energy difference between these sequences for a given level is compared with its experimental bandwidth.

CF Analysis of Nd^{3+} in the $AgNd(WO_4)_2$ Tetragonal $I\bar{4}$ Phase. The method used for calculating the energy levels of the Nd^{3+} $4f^3$ configuration assumes the central-field approximation. The total Hamiltonian consists of two parts, first that corresponding to the FI interactions, H_{FI}, and then the external effects represented by the CF arising from the influence of the surrounding charges of the crystalline lattice on the 4f electrons, H_{CF}. The FI part includes the spherically symmetric one-electron term of the Hamiltonian, the electrostatic repulsion between equivalent *f* electrons, the spin−orbit interaction, and terms accounting for higher-order corrections,[27] which for Nd^{3+} include up to 20 FI parameters

$$H_{FI} = H_0 + \sum_{k=0,1,2,3} E^k e_k + \zeta_{4f} A_{SO} + \alpha L(L+1) + \beta G(G_2) + \gamma G(R_7) + \sum_{k=0,2,4} M^k m_k + \sum_{i=2,4,6} P^i p_i + \sum_{\lambda=2,3,4,6,7,8} T^\lambda t_\lambda \quad (1)$$

The CF effect accounted for in the simulations includes only the standard one-electron part. The CF Hamiltonian[28] is expressed as a sum of products between the spherical harmonics C_q^k and the CF parameters B_q^k

$$H_{CF} = \sum_{k,q} B_q^k C_q^k \quad (2)$$

with $k = 2, 4, 6$ (with $|q| \leq k$). For Nd^{3+} occupying sites with the rather high S_4 symmetry in the tetragonal $AgNd(WO_4)_2$ host, the number of B_q^k is restricted to five real and one complex parameter, which must be adjusted to give the best overall agreement between the calculated and the observed Stark levels.

The selection of adequate sets of FI and CF parameters are the first steps of the fitting procedure. As starting values for FI parameters we used those of Nd^{3+} in $NaBi(WO_4)_2$.[26] Initial values for the six CF parameters were those calculated from crystallographic data applying the semi-empirical SOM.[29] The calculations have assumed Nd^{3+} in both the S_4 2b and 2d sites in the $AgNd(WO_4)_2$ host and the distances to their respective coordination oxygens. The two obtained sets of parameters are collected in the SOM columns in Table 2.

For the S_4 CF potential the Stark components of a $^{2S+1}L_J$ state of Nd^{3+} are characterized by crystal quantum numbers $\mu = \pm 1/2, \pm 3/2$, corresponding to the $\Gamma_{5,6}$ and $\Gamma_{7,8}$ IR, respectively, which must be assigned following the polarization rules for dipolar electric and dipolar magnetic transitions.[30] The IR of $^2P_{1/2}$ is $\Gamma_{7,8}$, and because the 5 K optical absorption transition is observed in the σ spectrum, the ground level from which this transition originates has also a $\Gamma_{7,8}$ IR. Accordingly, 5 K transitions from the ground Stark level to the $\Gamma_{7,8}$ levels will be observed in the σ spectrum, whereas those to the $\Gamma_{5,6}$ levels will be observed simultaneously in σ and π spectra. The 99 observed energy levels collected in Table 1 have been labeled with the σ or σ and π polarization character of the absorption transition and with the corresponding IR as discussed above.

The procedure followed in the fitting process is similar to that previously described and successfully used for other RE^{3+} in ordered[31,32] as well as in disordered[25−27,33] DT single crystals, with a simultaneous treatment of both FI and CF

(27) Rico, M.; Volkov, V.; Cascales, C.; Zaldo, C. *Chem. Phys.* **2002**, *279*, 73.
(28) Wybourne, B. G. *Spectroscopic properties of Rare Earths*; Wiley: New York, 1965.
(29) Porcher, P.; Couto dos Santos, M.; Malta, O. *Phys. Chem. Chem. Phys.* **1999**, *1*, 397.
(30) Görller-Walrand, C.; Binnemans, K. Rationalization of crystal-field parametrization. In *Handbook on the Physics and Chemistry of Rare Earths*; Gschneidner, K. A., Jr., Eyring, L., Eds.; North-Holland: Amsterdam, 1996; Vol. 23, p 121.
(31) Zaldo, C.; Rico, M.; Cascales, C.; Pujol, M. C.; Massons, J.; Aguiló, M.; Díaz, F.; Porcher, P. *J. Phys.: Condens. Matter* **2000**, *12*, 8531.
(32) Pujol, M. C.; Cascales, C.; Rico, M.; Massons, J.; Díaz, F.; Porcher, P.; Zaldo, C. *J. Alloys Compd.* **2001**, *323−324*, 321.
(33) Méndez-Blas, A.; Rico, M.; Volkov, V.; Cascales, C.; Zaldo, C.; Coya, C.; Kling, A.; Alves, L. C.; *J. Phys.: Condens. Matter* **2004**, *16*, 2139.

Table 2. FI and S_4 Average CF Parameters (cm^{-1}) for Nd^{3+} in the Tetragonal $AgNd(WO_4)_2$ Crystal[a]

	SOM		$AgNd(WO_4)_2$	$Nd:NaBi(WO_4)_2$
	2b(I)	2d(II)	S_4	C_2
E^0			23 492(2)	23 484(1)
E^1			4781.0(7)	4792(7)
E^2			23.10(1)	23.15(2)
E^3			481.72(7)	479.98(8)
α			21.79(3)	21.90(2)
β			−629(3)	−686(3)
γ			[1500]	[1500]
ζ			880.7(6)	890.4(6)
$M^{0,b}$			1.76(6)	2.05(6)
$P^{2,c}$			233(13)	27.75(13)
T^2			[340]	[348]
T^3			19(2)	30(2)
T^4			68(2)	93(2)
T^6			−295(4)	−283(5)
T^7			354(5)	326(6)
T^8			[335]	[331]
B_0^2	*715*	*697*	486(11)	386(18)
B_2^2				100(14)
B_0^4	*−904*	*−827*	−841(26)	−1011(33)
B_2^4				229(42)
S_2^4				−90(59)
B_4^4	*±939*	*±821*	±995(16)	−664(33)
S_4^4				−795(26)
B_0^6	*−281*	*−343*	−157(27)	−96(46)
B_2^6				−63(39)
S_2^6				−179(63)
B_4^6	*±1025*	*±951*	±774(20)	−717(23)
S_4^6	*±358*	*±185*	±250(30)	−363(32)
B_6^6				−68(45)
S_6^6				−98(44)
S_2^d	*320*	*312*	217	184
S_4	*521*	*475*	546	605
S_6	*433*	*392*	322	328
S_T	*433*	*399*	386	411
N_L			99	85
σ^e			12.6	13.6
residue			12 802.3	10 775.6

[a] Italics indicate CF parameters calculated from SOM ($\rho = 0.05$; effective charge for oxygen $= -0.8$) for 2b and 2d S_4 Nd^{3+} sites in $AgNd(WO_4)_2$. Values in parentheses refer to estimated standard deviations in the indicated parameter. Values in square brackets were not allowed to vary in the parameter fitting. FI and C_2 CF parameters for the isostructural Nd-doped $NaBi(WO_4)_2$ crystal[26] appear in the right column. [b] M^0, M^2, and M^4 were constrained as $M^2 = 0.5625M^0$, $M^4 = 0.3125M^0$. [c] P^2, P^4, and P^6 were constrained as $P^4 = 0.50P^2$ and $P^6 = 0.10\ P^2$. [d] $S_k = \{1/(2k+1)[(B_0^k)^2 + 2\sum_q[(B_q^k)^2 + (S_q^k)^2]]\}^{1/2}$ $S_T = [(1/3)\sum_k S_k^2]^{1/2}$. [e] $\sigma = [\sum(E_0 - E_c)^2/(N_L - N_P)]^{1/2}$, where N_L is the number of levels and N_P is the number of parameters.

effects conducted using the entire, untruncated basis set of Nd^{3+} wave functions.[34]

Taking into account the similarity between the two sets of calculated SOM CF parameters for Nd^{3+} in the 2b and 2d crystallographic sites, which moreover is expected from the very close nature of the cationic sites and the comparable distances to their coordination oxygens, both individual fits of the energy level scheme finally converge, in the limit of the estimated standard deviations, to a unique collection of final values. This simulation reproduces accurately the observed energy levels sequence, with a low $\sigma = 12.6\ cm^{-1}$. Final results of the refinement are summarized in Table 1 for the energy levels and in Table 2, the S_4 column, for FI and CF parameters. The confidence and physical meaning of the fit are indicated by the low σ value obtained, but even more important is that no large discrepancies between calculated and experimental values of individual levels are observed. Furthermore, they are also sustained by the assignment made of the IR to each observed energy level, the simultaneous treatment in the fitting procedure of FI and CF interactions, and the utilization of the complete basis set of wave functions for the $4f^3$ configuration.

Paramagnetic Susceptibility Simulations from CF Effects. The phenomenological parametrization of a given CF potential through accurately determined wave functions associated to the well-adjusted energy levels of RE^{3+} in solids is a well-proven tool for the interpretation not only of spectroscopic properties but also of some magnetic ones, namely, the thermal variation of the paramagnetic susceptibility χ, the magnetic moment μ, and the magnetic splitting factor g for each Kramers doublet for a RE^{3+} configuration with an odd number of electrons, all of them in each crystallographic direction.[35] This is done using the van Vleck formalism:[36]

$$\chi_i = N\beta^2\sum_a\left[\frac{\langle\phi_a|(L+g_eS)\mathbf{u}|\phi_a\rangle^2}{kT} - 2\sum_b\frac{\langle\phi_a|(L+g_eS)\mathbf{u}|\phi_b\rangle\langle\phi_b|(L+g_eS)\mathbf{u}|\phi_a\rangle}{E_a - E_b}\right]B_a \quad (3)$$

where N is Avogadro's number, β the Bohr magneton, k the Boltzmann constant, E and ϕ the nonperturbed by the magnetic field energy levels and wave functions, respectively, described on the $|SLJM_J\rangle$ basis and provided by spectroscopic measurements and CF analysis, and $L + g_eS$ is the component (i) of the magnetic interaction associated to a tensorial operator of rank 1, where the magnetic dipole operator, $g_e = 2.0023$, is the gyromagnetic ratio, being $\mathbf{u}$ the unitary vector corresponding to the i axis. The sums run over thermally populated levels, according to the thermal partition law $B_a = \exp(-E_a/kT)/\sum_a \exp(-E_a/kT)$. In this expression the matrix elements are calculated using the Racah algebra rules.

The formula is the sum of a temperature-dependent diagonal term and a temperature-independent off-diagonal term, which is reminiscent of the classical Curie−Weiss law. The off-diagonal term, a result of the second order perturbation, usually has little importance, with the exception of the ground states with $J = 0$ ($RE^{3+} = Eu$). The sum runs over all other states ($b \neq a$). Energy levels up to 5000 and 10 000 cm^{-1}, for the diagonal and off-diagonal terms, respectively, which are largely sufficient to cover the thermal population effect above 300 K, were accounted in the calculation along with the J mixing of the levels.

For the actual S_4 symmetry of Nd^{3+} in the single-crystal host, the anisotropic χ_i components are called $\chi_{||}$ (component 0 of the tensor) and $\chi_\perp$ (components ±1 of the tensor). They have been also calculated[34] on the basis of the wave functions from the FI and S_4 CF parameters of Table 2.

(34) Porcher, P. *Fortran routines REEL and IMAGE for simulation of d^N and f^N configurations involving real and complex crystal field parameters*, 1989

(35) Sáez-Puche, R.; Climent, E.; Romero de Paz, J.; Martinez, J. L.; Monge, A.; Cascales, C. *Phys. Rev. B* **2005**, *71*, 024403.

(36) van Vleck, J. H. *J. Appl. Phys.* **1968**, *39*, 365.

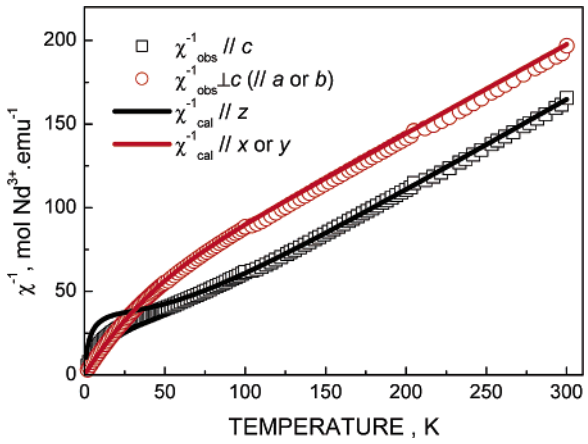

Figure 9. Comparison between experimental (symbols) and calculated (lines) curves of the thermal variation of χ_m^{-1} for the $AgNd(WO_4)_2$ single crystal.

The experimental curves of the molar χ versus T measured along parallel $\chi_{||}$ and perpendicular $\chi_\perp$ directions to the c crystal axis of $AgNd(WO_4)_2$ have been plotted in Figure 9. Taking into account that both 2b and 2d Nd^{3+} sites have the $\bar{4}$ inversion axis in the same tetragonal primary [001] crystal direction, measured $\chi_{||}$ corresponds to the mean S_4-calculated χ along the z direction for Nd^{3+} sites, χ_z, and measured $\chi_\perp$ to mean calculated χ_x or χ_y.

It can be observed that above ~25 K that $\chi_{||}$ values are higher than the $\chi_\perp$ ones, and the paramagnetic susceptibility obeys a Curie−Weiss law in a wide range of temperatures ~ 55−300 K. Magnetic susceptibility curves calculated (eq 3) using S_4 CF parameters of Table 2 reproduce adequately the experimental values, with excellent concordances for temperatures from 45 K up to 300 K, and the crossing of the $\chi_{||}$ and $\chi_\perp$ curves is also quite well-simulated. The bending at low temperature of the $\chi_\perp$ curve is especially well-reproduced, although some incertitude in the determination of CF parameters, maybe related to a *real* small distortion in the close-range local S_4 Nd^{3+} environments, is slightly affecting the reproduction of low-temperature $\chi_{||}$.

Therefore, the optimized set of FI and CF parameters achieved for tetragonal $AgNd(WO_4)_2$ crystal in Table 2 describes correctly the experimental optical and anisotropic paramagnetic susceptibility results for Nd^{3+}.

Influence of the CF on the Bandwidth. To describe the contribution of the two Nd^{3+} S_4 crystal sites in the observed line width of GSA transitions ΔE_0, we have calculated two series of $4f^3$ energy levels using the optimized FI parameters of Table 2 and the SOM derived CF parameters for the 2b and 2d sites, also in Table 2. The energy difference between equivalent levels originated from these two sites, ΔE_c, can be found in Table 1. Generally, $\Delta E_c \leq \Delta E_0$, supporting that although the individual line profiles of these two centers were not resolved in the experimental 5 K GSA measurements, they are a major contribution to the observed bandwidths.

From the comparison between previously reported C_2 CF parameters for the also tetragonal $I\bar{4}$ Nd-doped $NaBi(WO_4)_2$[26] with current S_4 CF results for the $AgNd(WO_4)_2$ single crystal, Table 2, it can be established that despite of differences in the symmetry around Nd^{3+} centers, the strength of the local CF around Nd^{3+} centers is in both cases very similar. In fact, S_4 magnitudes are the more important ones, and the described C_2 local distortion for Nd-doped $NaBi(WO_4)_2$ is quantitatively of small importance, that is, the CF parameters involved in the distortion are small, even negligible, mainly B_2^k (k = 2, 4), which are related to the close-range coordination around Nd^{3+}.

IV. Conclusions

Two RT stable phases can be achieved for $AgNd(WO_4)_2$: (i) polycrystalline powders prepared by annealing in the 800−1164 °C range or single crystals grown by the Czochralski method at 1164 °C adopt the symmetry of the tetragonal SG $I\bar{4}$ (No. 82) and (ii) polycrystalline powders synthesized below 800 °C possess the monoclinic symmetry of the SG $C2/m$ (No. 12). These phases have quite different colors. As a result of the nearly nonreversible monoclinic to tetragonal transformation, the color phase can be used to evidence overheating events. Nd^{3+} are located on a single C_{2v} crystal site in the $C2/m$ host, while two S_4 crystal sites, 2b and 2d, randomly shared with Ag^+ cations, are occupied by Nd^{3+} cations in the tetragonal $I\bar{4}$ phase; thus, several different local cationic environments around each one of these two sites can be envisaged. Nd^{3+} cations experience a more intense and anisotropic CF, and consequently larger splitting for $^{2S+1}L_J$ multiplets, in the monoclinic phase than in the tetragonal disordered one. Moreover, bandwidths of low-temperature optical transitions are up to four times larger in the tetragonal phase. Despite this broadening, Nd^{3+} centers remain with well-defined relative orientations, exhibiting polarization rules featuring the S_4 symmetry, which allows the analysis and parametrization of CF effects conducted with corresponding IR for each energy level. The correctness of the results is assured through the successful reproduction of the thermal evolution of the anisotropic paramagnetic susceptibility in a $AgNd(WO_4)_2$ single crystal. On the basis of the CF analysis it is concluded that the two Nd^{3+} sites are contributing inside the experimental bandwidth, despite that they are not currently resolved in 5 K GSA experiments.

Acknowledgment. The authors acknowledge the financial support through the Spanish Projects Nos. MAT2002-04603-C05-05, CAM MAT/0434/2004, and MAT 2003-08465-C02-01 and also from the European Commission, Project No. DT-CRYS, UE NMP3-CT-2003-505580.

CM051789L